



ISSN: 2617-6548

URL: www.ijirss.com



A new-generation approach to PAM-4 Based on the Fano resonance effect using a multimode interference structure

 The Duong Do¹,  Thanh Nhat Hoang²,  Duy Tien Le³,  Trung Thanh Le^{4*}

¹University of Transport and Communications, Hanoi, Vietnam.

^{2,3,4}International School, Vietnam National University, Hanoi, 144 Xuan Thuy, Cau Giay, Hanoi, Vietnam.

Corresponding author: Trung Thanh Le (Email: thanh.le@vnu.edu.vn)

Abstract

The goal of this research is to come up with a new optical structure for the generation of multilevel pulse amplitude modulation (PAM-4) signalling, which is used for optical interconnects and data center networks. The Fano effect is made with a structure made up of a 4x4 MMI coupler, feedback waveguides, and phase shifters. For the production of PAM-4, we employ the Fano effect. The new proposed approach can reduce power consumption and extend the linear region of the device transfer function compared with conventional approaches based on Mach Zehnder Interferometers (MZI) and ring resonators. We show that an extreme reduction of power consumption of 3 to 30 times, compared with the conventional structure based on MZI and ring resonators, is achieved. In addition, the proposed structure based on silicon wave guides has the advantages of extreme high bandwidth, large fabrication tolerance, and a compact footprint. The proposed structure can be applied to generate the PAM-4 based on the Fano effect with low power consumption, and it is suitable for complex systems with a lot of transceivers. The device is numerically simulated and designed using the Finite Difference Method (FDM) and Finite Difference Time Difference (FDTD). The PAM-4 structure based on silicon waveguides can be compatible with CMOS's existing technologies.

Keywords: Data center networks, Integrated optics, Micro ring resonator, Multi-level modulation, Multimode interference (MMI), Optical interconnects, Silicon photonics.

DOI: 10.53894/ijirss.v6i4.2120

Funding: This research is supported by Vietnam National Foundation for Science and Technology Development (Grant number: 103.03-2018.354).

History: Received: 18 December 2022/**Revised:** 27 June 2023/**Accepted:** 20 September 2023/**Published:** 02 October 2023

Copyright: © 2023 by the authors. This article is an open access article distributed under the terms and conditions of the Creative Commons Attribution (CC BY) license (<https://creativecommons.org/licenses/by/4.0/>).

Authors' Contributions: All authors contributed equally to the conception and design of the study. All authors have read and agreed to the published version of the manuscript.

Competing Interests: The authors declare that they have no competing interests.

Transparency: The authors confirm that the manuscript is an honest, accurate, and transparent account of the study; that no vital features of the study have been omitted; and that any discrepancies from the study as planned have been explained. This study followed all ethical practices during writing.

Institutional Review Board Statement: Not applicable.

Publisher: Innovative Research Publishing

1. Introduction

The utilization of higher modulation schemes is a potential strategy for attaining enhanced bandwidth efficiency. In the literature, on-off keying (OOK) is frequently used for optical transmission in optical interconnects and data center networks [1, 2]. However, systems based on OOK have a limited bit rate and complexity. To increase the bit rate, higher modulation can be employed, with PAM-4 (4-level pulse amplitude modulation) being a suitable candidate [3]. In recent years, PAM-4 in the optical domain has gained attraction due to its simple requirement of digital signal processing (DSP) techniques [4, 5]. OOK built on the Mach-Zehnder interferometer can achieve PAM-4. However, these structures exhibit low linearity, and the primary focus of current research is to enhance the linearity of the MZI for PAM-4.

To meet the growing demand for higher bit rates in optical communication and interconnect systems, we need to improve spectral efficiency by switching from on-off keying to higher modulation formats like PAM-N and N-QAM (Multilevel Quadrature Amplitude Modulation). PAM-4 is one potential modulation method where data is modulated using two levels of signal amplitude, offering the advantage of direct detection [6]. Multilevel amplitudes can be achieved by employing electrical digital-to-analog converters (DAC) [6] to drive either vertical-cavity surface-emitting lasers (VCSEL) or Mach-Zehnder interferometers [7]. However, these structures have drawbacks such as the generation of imposed chirp in directly modulated lasers (DML) and the challenge of designing high-frequency linear operating DACs. Another approach for converting binary streams into two levels involves using all-optical DACs, which can be realized using segmented phase shifters in the MZI. By employing suitable phase shifter designs, the total length of the phase shifter can be reduced [8]. However, these designs still rely on directional couplers, which make it difficult to minimize device footprint while maintaining fabrication tolerance and high bandwidth [9]. Although optimizing phase shifter design is a promising method for reducing device footprint, in this research, we propose a new approach that utilizes multimode interference couplers to achieve footprint reduction. Additionally, using the Fano effect can lower power consumption. We utilize the push-pull-driven MZI, enabling long-haul transmission system operation without generating chirp.

To save even more power in optical transmission systems, it has been suggested that the PAM-4 signal could be made without using electrical DAC or DSP techniques like pre-emphasis, pulse shaping, equalisation, etc. These methods have been achieved by using various modulator structures [10-12], such as MZIs with microring modulators [13], traveling wave modulators, dual microring resonators [14], segmented microring resonators [15], and push-pull segmented MZIs [16]. It should be noted that the device is driven by 4-level signals; there are no DAC or DSP techniques used in the transmission links. The electrical signals are achieved by combining two signals from a pulse pattern generator. In order to generate an optical PAM-4 signal, there are some methods, such as PAM-4 generation using microring resonators and Mach Zehnder Modulators (MZM) [17]. The drawbacks of these structures are their high power requirements. In addition, because the previous structures used directional couplers as coupling elements, it was difficult to achieve the required coupling ratios. The linear region of the transfer function of MZM and microring resonator structures is also limited. As a result, the eye opening of the PAM-4 signal when using the conventional structure is also narrow.

In recent years, microring resonators (MRRs) have emerged as versatile components in on-chip interconnects and photonic integrated circuits [18]. The creation of Fano resonance through MRR structures has garnered significant attention, particularly for on-chip integrated functions [19]. Unlike the symmetric Lorentzian resonance exhibited by single MRRs, Fano resonance provides asymmetric and sharp slopes. The narrow wavelength range for tuning transmission from zero to one in Fano lineshapes offers favorable characteristics such as low power consumption, high sensing sensitivity, and a high extinction ratio [20]. Fano resonance is a well-known phenomenon in physical waves, arising from the interference between continuum and discrete localized states [21]. In photonics, Fano resonances can be generated by coupling MRRs with Mach-Zehnder interferometers or Fabry-Perot cavities, considering resonant modes in MRRs as discrete states. The generation of Fano resonance is a topic of great interest due to its applications in high-sensitivity sensing, low-power switching, low-power modulation, and fast-slow light generation [22, 23]. Fano resonance exhibits an asymmetric lineshape, while Mach-Zehnder interferometers generate a symmetric lineshape [22]. The slope rate of Fano resonance is much higher than that of the MZI [24], enabling low-power operation in modulation and switching based on Fano resonance. Various methods have been proposed for generating Fano resonances, such as photonic crystals, plasmonic structures, metamaterial structures, Bragg gratings, air hole resonators [25], and microring resonators [26]. However, most of the existing methods for generating Fano resonance using microring resonators rely on directional couplers. In this research, we introduce a novel approach to realize Fano resonance based on the multimode interference effect in multimode waveguides with a feedback waveguide. Previous studies have explored Fano-like resonances in photonics using configurations involving cavities and partially transmitting elements (PTE) coupled systems [27], ring and Mach-Zehnder interferometer (MZI) coupled systems [28], 2D photonic crystal cavities, or coupled 2D photonic crystal cavities [29]. Many of these approaches require complex fabrication technologies, such as electron-beam lithography for patterning photonic crystals. For silicon photonics foundries to be able to use CMOS-compatible processes or DUV (deep ultraviolet) lithography, it is very important to show that devices with Fano-like resonances can be made that are small, have low loss, have a wide bandwidth, are easy to make, and are compatible with CMOS technology [29, 30].

Therefore, we present a new architecture to generate an optical PAM-4 signal based on the Fano resonance. Our structure can generate the Fano effect, which is used for PAM-4 signalling, to solve the above limitations. The proposed structure can provide a high bandwidth and low fabrication tolerance due to the use of a multimode interference coupler with the feedback waveguides. The whole device is simulated and designed using the existing CMOS technologies for silicon photonics [31, 32]. Due to their compatibility with the existing Complementary Metal Oxide Semiconductor (CMOS), silicon waveguides are used for photonic integrated circuits. The advantages of silicon waveguides are low loss, low cost, and compact size.

2. Silicon Photonic PAM-4 Structure Based on an MMI with a Microring Resonator

Figure 1 a presents the proposed structure for PAM-4 generation, where an MMI coupler is used for a microring resonator with the feedback waveguide. For a 4x4 MMI coupler, we use only input ports 1 and 3 (E_{in} and E_{out}). In our design, the silicon-on-insulator (SOI) rib waveguide and the plasma effect on the PN junction are used for the phase shifts.

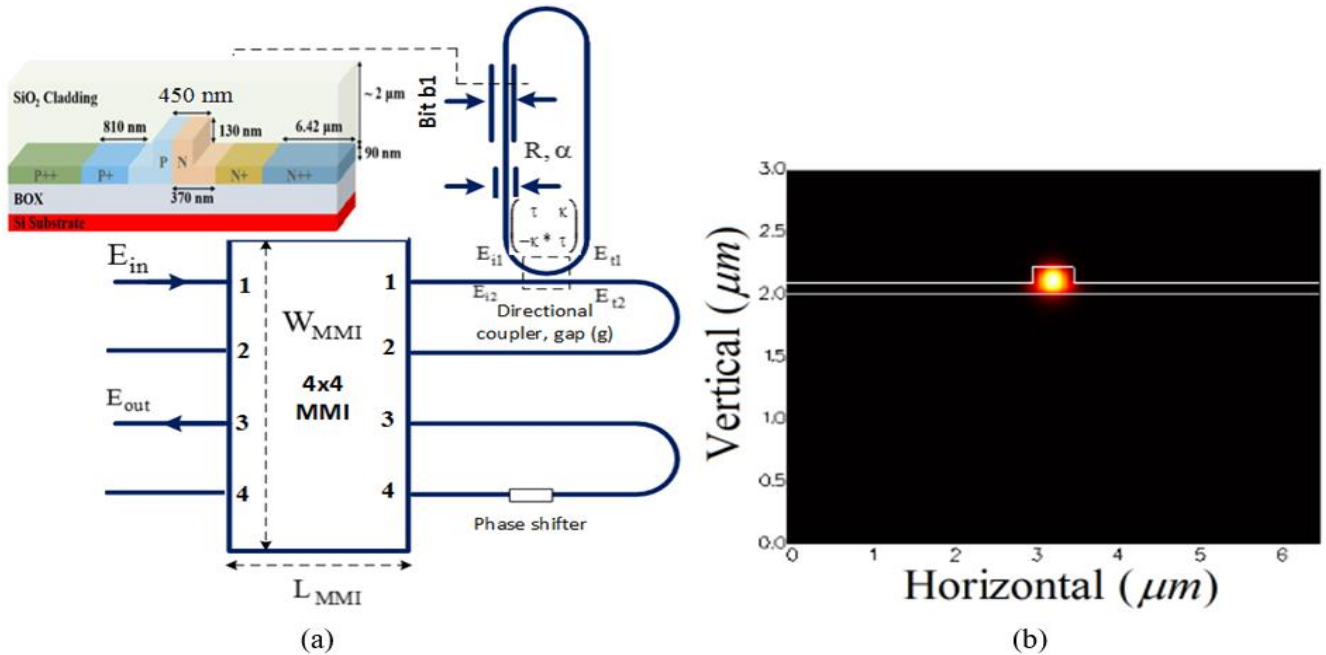


Figure 1.

(a) The proposed structure for optical PAM-4 generation, (b) fundamental mode of the SOI rib waveguide calculated by the Finite Difference Method (FDM).

Note: * indicates the complex conjugate.

In order to create the micro ring resonators, two feedback waveguides are used. The rib SOI waveguide has a width of 450nm and a height of 220nm for single-mode operation. The slab height is 90nm. At a wavelength of 1550nm, the refractive index of Si, $n_{Si}=3.45$ and the refractive index of SiO₂, $n_{SiO_2}=1.5$. Two shifters are used for two bits b_0b_1 to generate 4 levels of PAM-4. We use the plasma effect on the PN (N- type and P-type semiconductor) junction for phase shifters. The width W_{MMI} and the length L_{MMI} of the 4x4 MMI coupler and the positions of the input and output waveguides are selected carefully to achieve the required Fano resonance. The Fano resonance can provide a steep slope and linear region. We use this property to achieve the device with smaller power consumption compared to the conventional structures based on ring resonators and MZMs. By using the Finite Difference Method (FDM), the mode profile of the optical waveguide at 1550nm is shown in Figure 1b. The effective refractive index is calculated to be $n_{eff} = 2.61$. For the phase shifter designs, we use the structure given by Samani, et al. [33] for optimal low losses. For optimal design, we use the phase shifter with 6 doped regions as given in the reference [34].

There are two phase shifter regions with the lengths of L_1 and L_2 , where $L_2 = 2L_1$, applied voltage V_1 and V_2 respectively. The phase shifter having length of L_1 is used for least significant bit (LSB) and L_2 is for Maximal Significant bit (MSB) of input data bits b_0b_1 . In this research, phase shifter in silicon photonic platform is based on the plasma dispersion effect. The phase shift is created by changing of the refractive index of silicon waveguides, which can be changed by changing the carrier doping in the waveguide. Therefore, to achieve phase-shift in silicon waveguide, PN junctions are embedded in silicon waveguide by doping the waveguide. By applying an electrical external voltage to the PN junction and driving it to depletion or injection mode, the refractive index of the silicon waveguide changes and as a result, the group velocity of the optical wave travelling in the silicon waveguides changes. By implementing the PN doped silicon waveguides, the Mach-Zehnder interferometer structure with amplitude modulation can be achieved. It is noted that doping the silicon waveguides results in higher optical losses. The change in refractive index at 1550 nm wavelength formulated by Soref and Bennet can be expressed as follows [35]:

$$\Delta n = -5.4 \times 10^{-22} \Delta N^{1.011} - 1.53 \times 10^{-18} \Delta P^{0.838} \quad (1)$$

$$\Delta \alpha = 8.88 \times 10^{-21} \Delta N^{1.167} + 5.84 \times 10^{-20} \Delta P^{1.109} \quad (2)$$

Where ΔN and ΔP are carrier concentrations of electrons and holes, respectively. The research focused on optimizing the doping concentrations in silicon waveguides to obtain high modulation efficiency and low loss. Six different doped concentrations are now available in the process offered by the foundry services. In the case of modulators that have a silicon waveguide, when subjected to a voltage, the figure of merit (FoM) varies non-linearly due to the non-linear change of the Si refractive index. In this way, the modulation efficiency can be calculated according to Dourado, et al. [36].

$$\Delta n_{\text{eff}} = \frac{\iint (n_{s_i} + \Delta n(x, y)) |E(x, y)|^2 dx dy}{\iint |E(x, y)|^2 dx dy} \tag{3}$$

Equation 3 presents the effective index change due to the plasma effect. Multimode interference (MMI) is based on the idea that if you make a single-mode waveguide thicker, multiple higher-order modes can travel through it and interfere with each other. Because each mode moves at a different speed and the energy in higher-order modes is spread across multiple nodes laterally, this component can be used to split signals into N separate paths (NxN). As a consequence of the interference between different modes, z-dependent lateral standing wave profiles are obtained. By carefully selecting the length of the MMI, a high electrical field node within it can be directed as a single guided mode in the output waveguides. MMIs are easier to manufacture compared to directional couplers, which require sub-mm gaps, as they possess a higher tolerance for dimensional variations during the fabrication process compared to most other optical couplers. Moreover, this component exhibits inherent advantages such as low loss and wide optical bandwidth. One limitation of ordinary MMIs arises from rear reflections, which utilize the same self-imaging principle observed in the forward direction of the MMI. However, this drawback can be addressed through clever design alterations, such as introducing slanted input and output sidewalls instead of completely straight configurations. The multimode interference (MMI) device is a wide rectangular waveguide. To solve for the electric field in the waveguide, the field in the MMI waveguide can be expressed by Okamoto [37]:

$$\frac{d^2 E(x)}{dx^2} + [k^2 n^2(x) - \beta^2] E(x) = 0 \tag{4}$$

Where k is the free-space wavenumber. The important thing is to design the 4x4 MMI coupler to achieve the desired matrix property to create the Fano effect. We use the MPA (mode propagation analysis) and numerical simulation based on the Finite Difference Time Difference (FDTD), and the locations of the input and output waveguides of the MMI are $x_i = (i + \frac{1}{2}) \frac{W_{\text{MMI}}}{N}$ (i=0, 1, 2, 3). The field of the MMI coupler can be written by Heaton and Jenkins [38].

$$E(x, z) = \exp(-jkz) \sum_{m=1}^M E_m \exp(j \frac{m^2 \pi}{4\Lambda} z) \sin(\frac{m\pi}{W_{\text{MMI}}} x) \tag{5}$$

Equation 5 presents the field within the MMI region. When considering 4x4 MMI couplers, it is necessary to carefully design and select the positions of the input and output waveguides, along with their specific lengths, in order to achieve the desired characteristic matrix. The analytical design of MMI couplers follows the principles outlined above and is relatively straightforward. However, there is currently no universally applicable approach that guarantees optimum performance for MMI couplers. As a result, it is important to investigate the impact of various parameters on the characteristics of MMI couplers using numerical methods.

In this study, the optimization of MMI couplers focuses on analyzing the effects of specific geometrical parameters. These parameters include the width and length of the MMI coupler itself, as well as the position and width of the input and output waveguides. By studying the influence of these parameters, we aim to enhance the performance and effectiveness of MMI couplers. From the numerical simulations, the desired MMI coupler with special length, width, and positions of input and output waveguides can be achieved [39]. We found out that the lengths of the MMI coupler are 6µm and 225µm, respectively [40]. The field propagations through the optimal 4x4 MMI coupler calculated by the Finite Difference Time Difference are shown in Figure 2. The mode profile is studied by the Finite Difference Method (FDM). Figure 2 shows the propagation going over the MMI coupler for input signals at ports 1 and 2. Two 3dB couplers can be achieved.

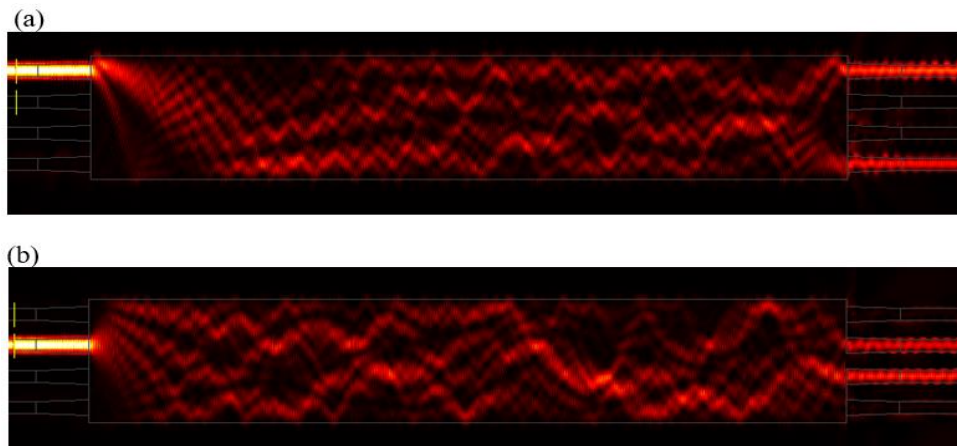


Figure 2. Optical field transmission over the MMI coupler for different input signals (a) input signal at port 1 and (b) at port 2.

In this research, we show that high bandwidth and large fabrication tolerances can be achieved. Figure 3 shows the simulation results for normalized output powers at ports 1 and 4 for different widths, lengths, and wavelengths. The simulation results show that fabrication tolerances in width of $\pm 10\text{nm}$ and in length of $\pm 500\text{nm}$ for 10% variation powers are obtained. These fabrication tolerances are feasible with the existing CMOS technology [41]. The -1dB bandwidth is calculated to be 20nm.

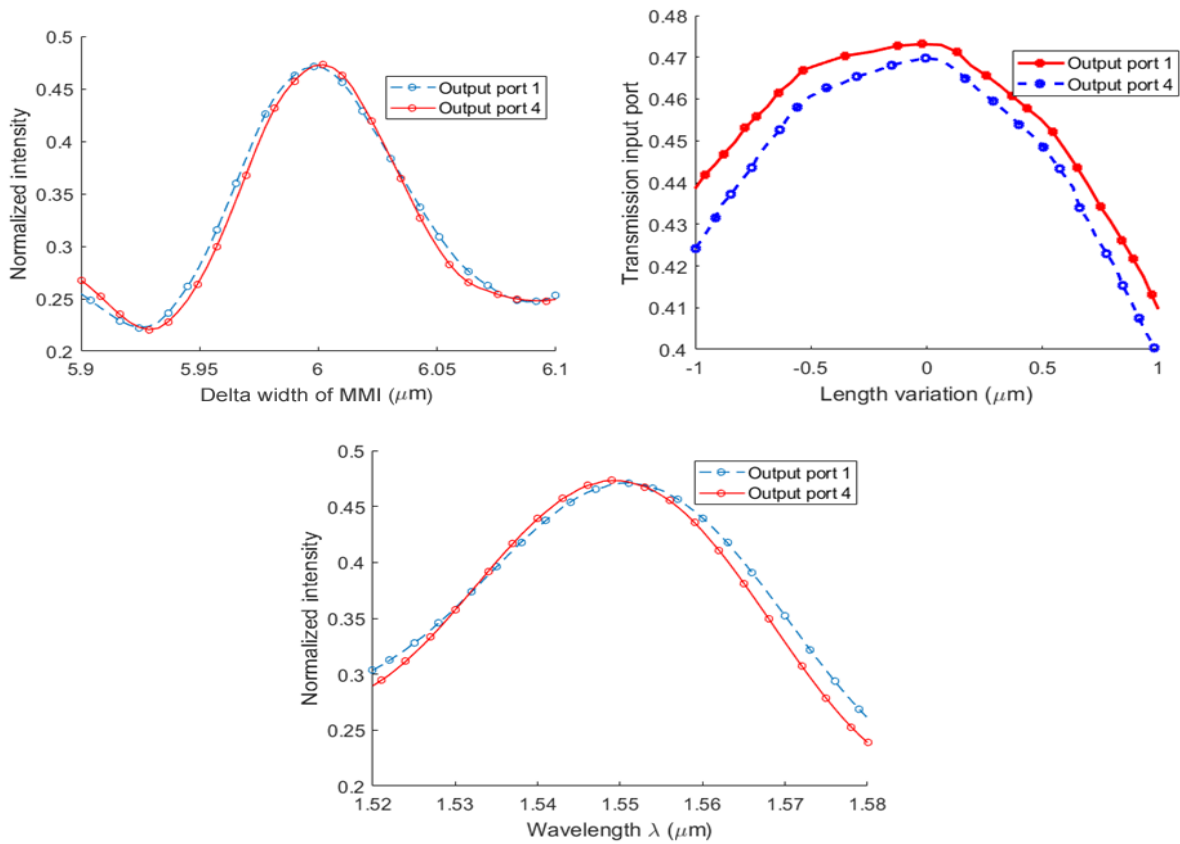


Figure 3. Output signals at port 1 and 3 of the MMI coupler at (a) different locations of the outputs, (b) different length (variation) and (c) wavelength.

By using the transfer matrix method, the fields at output of the single ring resonator in Figure 1 a is expressed by Yariv [42]:

$$\begin{pmatrix} E_{t1} \\ E_{t2} \end{pmatrix} = \begin{pmatrix} \tau & \kappa \\ -\kappa^* & \tau \end{pmatrix} \begin{pmatrix} E_{i1} \\ E_{i2} \end{pmatrix} \quad (6)$$

Where κ and τ are the cross coupling and transmission coupling coefficients of the coupler; $E_{i2} = \alpha \exp(j\varphi)E_{t2}$, α is the loss factor and L_R is the length of the ring waveguide. The loss factor of the ring waveguide can be calculated by:

$$\alpha = \exp(-0.5\alpha_{PS}L_{PS}) \exp[-0.5\alpha_{Si}(2\pi R - L_{PS})] \quad (7)$$

Where R is the radius of the ring waveguide and $\alpha_{Si} = 0.1 - 0.4\text{dB/cm}$ is the loss coefficient of the Si rib waveguide [43]. L_{PS} is the loss due to the phase shifters based on PN doped regions. From (2) and relation between E_{i2} and E_{t2} , the relation between the output and input fields of the ring resonator is expressed by:

$$E_{t1} = E_{i1} \frac{-\alpha + \tau e^{-j\varphi}}{-\alpha\tau^* + e^{-j\varphi}} \quad (8)$$

Where φ is the phase shift, which includes both the phase shift of the waveguide $\varphi_0 = 4\pi^2 n_{\text{eff}} \frac{R}{\lambda}$ and the phase shift due to the segmented phase shifters for PAM-4 generation? The output field of the device can be calculated by:

$$E_{\text{out}} = \frac{1}{2} E_{\text{in}} \left(\frac{-\alpha + \tau e^{-j\varphi}}{-\alpha\tau^* + e^{-j\varphi}} + e^{-j\theta} \right) \quad (9)$$

Where θ is the phase shift at the arm connected between output ports 3 and 4?

In order to accumulate the phase shift of the micro-ring resonator into the overall transmission of the device, we carefully designed the micro ring resonator to work in the over-coupled region [44]. The transmissions of the device and phase difference are shown in Figure 4. We can see that the Fano effect with the highest on-off ratio (maximal difference between two peaks) is achieved if the over-coupled requirement is met.

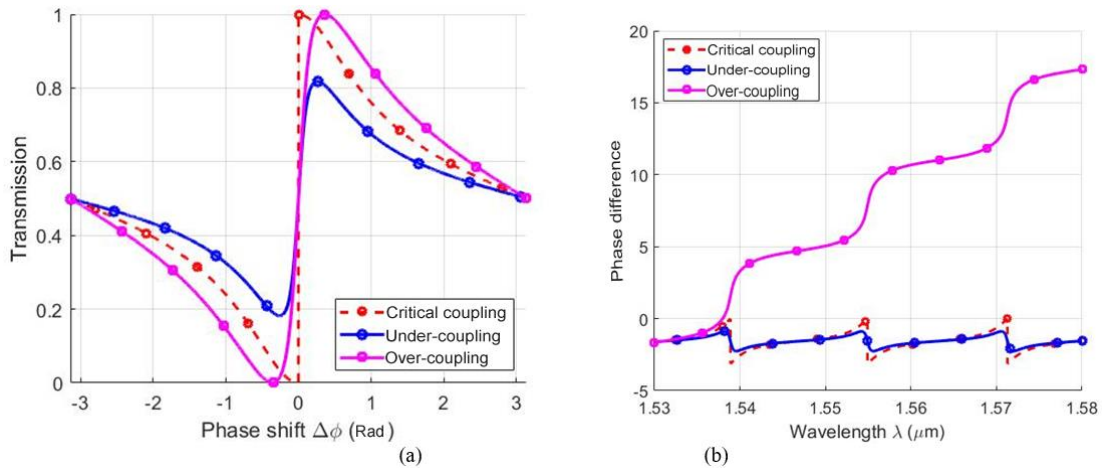


Figure 4.
(a) Transmissions and (b) phase shifts of the device at critical coupling, under-coupling and over-coupling condition.

In order to get the required coupling and transmission ratios κ, τ , the directional coupler of the micro-ring resonator needs to be carefully designed. The FDTD simulation shows that for a micro-ring radius of $R=5 \mu\text{m}$, the power coefficient $|\tau|^2$ can be expressed by an approximation of a curve with a polynomial $|\tau|^2 = -1.4368\lambda + 2.8362$; the refractive index of silicon material is used in theoretical simulations (transfer matrix method) by using the Sellmeier equation:

$$n^2(\lambda) = \varepsilon + \frac{A}{\lambda^2} + \frac{B\lambda_1^2}{\lambda^2 - \lambda_1^2} \quad (10)$$

Where $e = 11.6858$, $A=0.939816\text{mm}^2$, $B=8.10461 \times 10^{-3}$ and $l_1 = 1.1071\text{mm}$.

Figure 5 shows the FDTD simulations for the design of the directional coupler used in the ring resonator of Figure 1 a. The coefficient of the directional coupler depends on the gap between two waveguides and the radius. For the previous architectures of PAM-4 based on only one micro-ring resonator, the directional coupler had a great effect on the performance and working principle of the device [17, 45]. In this study, we only need the over-coupled condition to generate the Fano effect. The transmission of the proposed device is not significantly affected if the over-coupled condition is met, as shown in Figure 6.

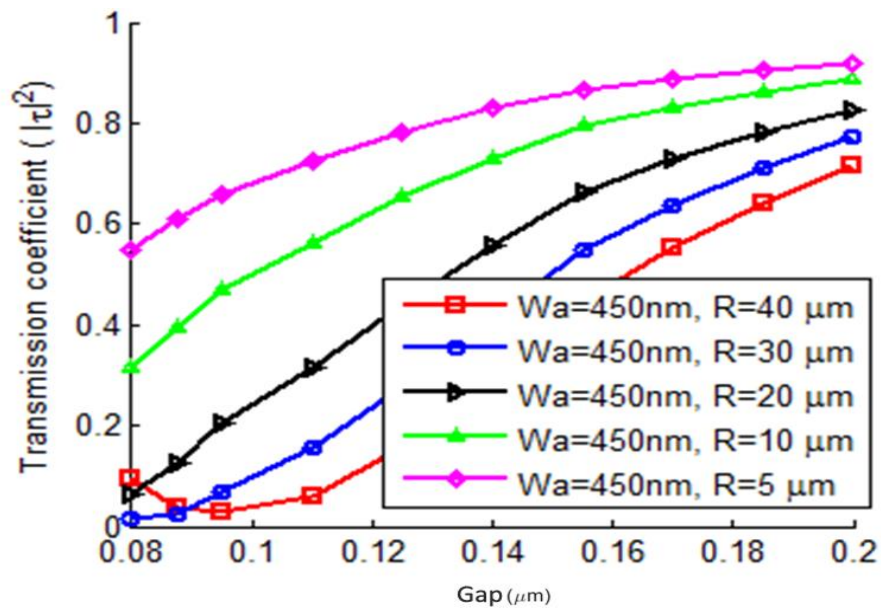


Figure 5.
Transmission coefficient at different gaps with different waveguide widths.

Figure 6 shows the simulations of the normalized transmissions at different waveguide loss factors inside the micro-ring resonator. We can see that the coupling ratio has a great effect on the working principle of the PAM-4 generation based on the Fano effect. By controlling the coupling coefficient ratios, the desired levels of PAM-4 can be obtained with lower power consumption.

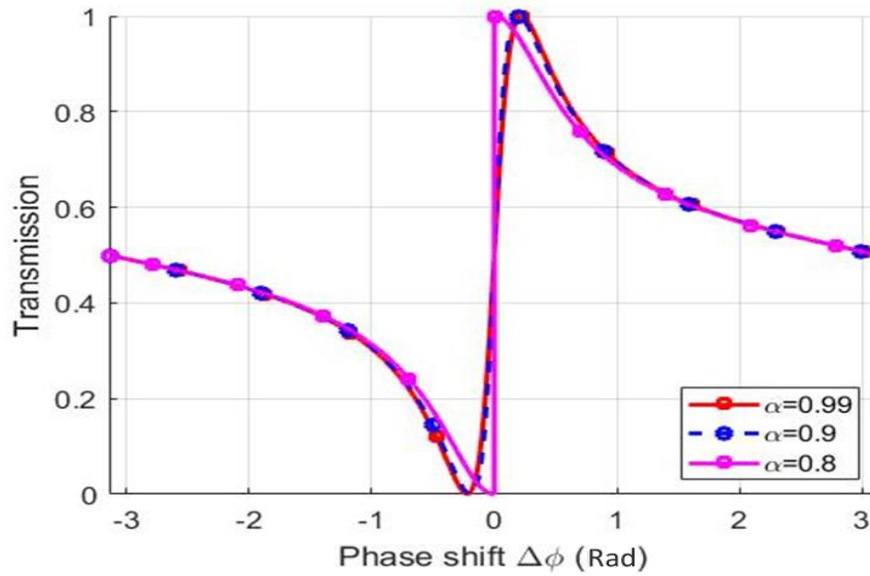


Figure 6.
Transmissions at different loss factor for an over-coupled condition.

For PAM-4 generation, we use four levels at 0.2, 0.4, 0.6, and 0.8 in normalized output powers, as shown in Figure 7. Figure 7 b presents the comparison for the PAM-4 generation using the MZM and the proposed Fano effect structure in this research. From the simulation results, the phase difference between two arms was calculated to be -0.06π , -0.02π , 0.02π , and 0.06π (rad), respectively, for bits 00, 01, 10, 11 of the 4 levels of PAM-4. From these simulation results, we see that a power consumption reduction of 3 to 30 times can be achieved compared with MZM structures used for PAM-4.

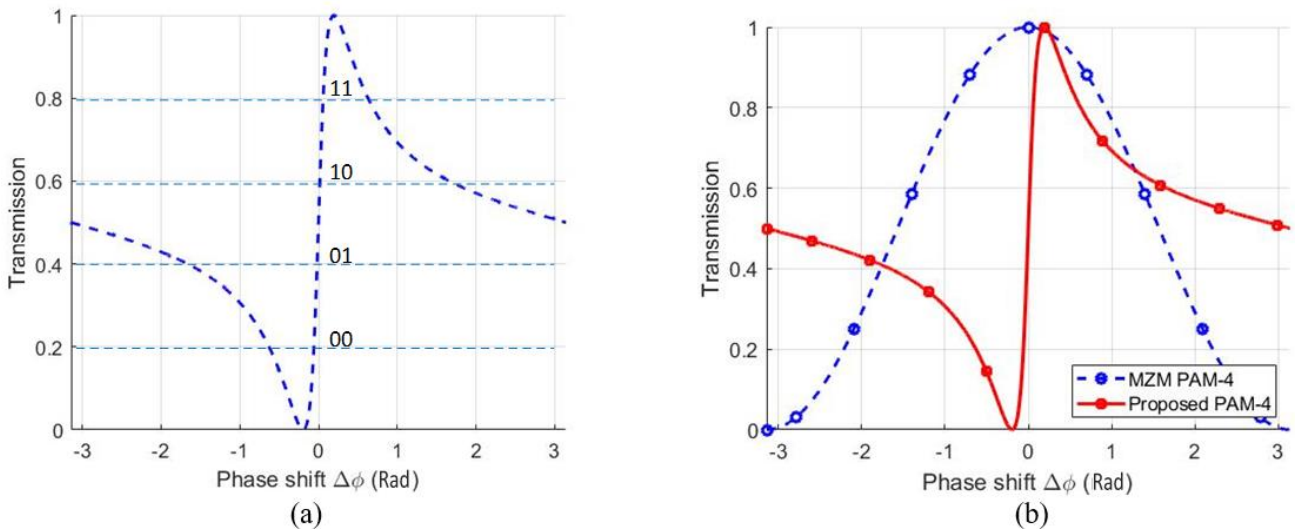


Figure 7.
(a) PAM-4 levels based on the Fano effect transmission and (b) The PAM-4 levels based on MZM and Fano effect.

Table 1 presents the phase shifts required for the PAM-4 signal using the MZM and the proposed structure. Figure 8 shows the comparison between two structures.

Table 1.
PAM-4 levels based on two segmented phase shifters.

PAM-4 bits	PAM-4 levels	Phase shifts if using the MZM	Phase shifts for this work
00	V0 (0.2)	2.23π rad	-0.06π rad
01	V1 (0.4)	1.77π rad	-0.02π rad
10	V2 (0.6)	1.37π rad	$+0.02\pi$ rad
11	V3 (0.8)	0.92π	$+0.06\pi$ rad

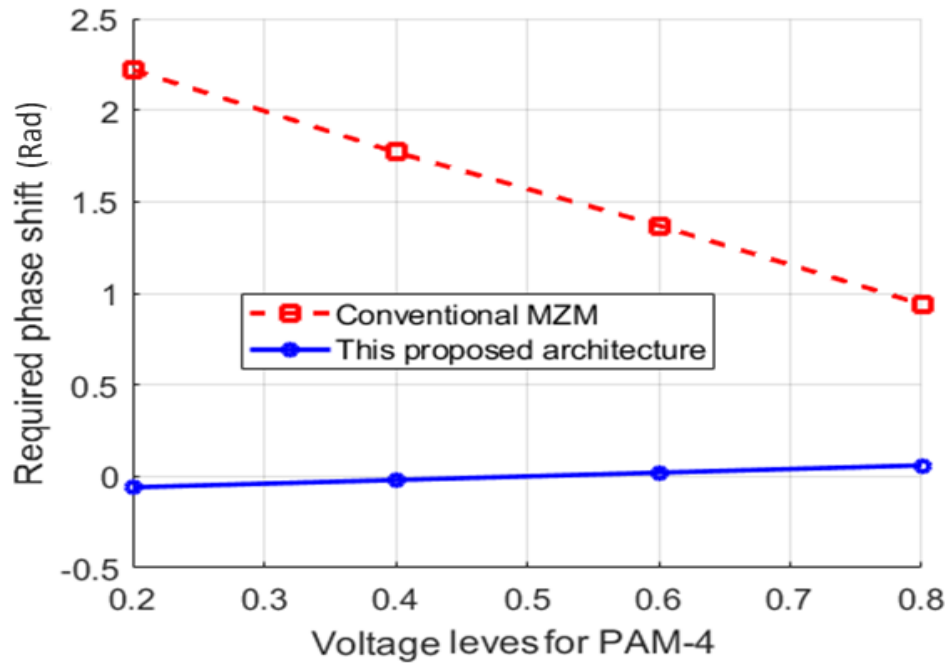


Figure 8.
Phase shifts required for PAM-4 with MZM and the proposed structure.

Finally, we use the FDTD simulation to verify the working principles of the proposed structure. The FDTD simulations for bits 00, 01, 10, 11 with 4 levels of PAM-4 are presented in Figure 9. The FDTD simulation parameters are: Gaussian pulse width of 15fs is used for input signal. The grid of the dimensions are $\Delta x = \Delta y = 5 \text{ nm}$ and $\Delta z = 10 \text{ nm}$.

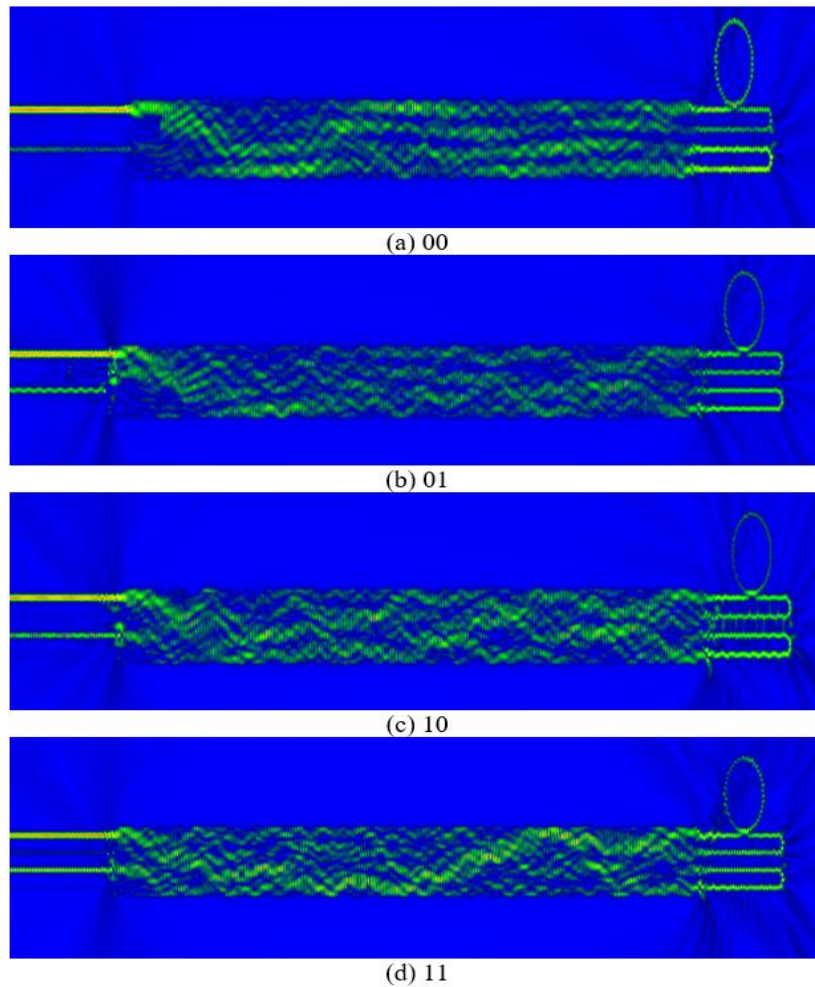


Figure 9.
FDTD simulation of the proposed device.

3. Conclusions

In this study, we have introduced an innovative approach for the implementation of PAM-4 modulation. Our technique utilizes Fano resonance, which is formed from a single 4x4 multimode interference (MMI) coupler with an over-coupled ring resonator. Notably, our approach is built upon complementary metal-oxide-semiconductor (CMOS) technology. The suggested structure demonstrates a notable Fano resonance, which facilitates a substantial decrease in power consumption for PAM-4 production. The reductions seen range from 3 to 30 times. In addition, the design offers a fabrication tolerance in width and length of $\pm 10\text{nm}$ and $\pm 500\text{nm}$, respectively, and a -1dB bandwidth of 20nm. This design is particularly suitable for photonic integrated circuits. The proposed approach has significant potential for utilization in the domains of high-performance computing, multicore systems, and high-speed data centers, where the efficient and dependable transfer of data bears utmost importance. By capitalizing on the advantages of Fano resonance and harnessing the capabilities of our suggested structure, it is possible to improved performance and energy efficiency in these challenging systems. The architecture exhibits a high level of compatibility with photonic integrated circuits.

References

- [1] I. Task_Force, "200 Gb/s and 400 Gb/s ethernet task force," Retrieved: <https://www.ieee802.org/3/bs/index.html>. [Accessed 10-2-2022], 2022.
- [2] J. Wang, "Optical PAM-4 generation via electromagnetically induced transparency in nitrogen-vacancy centers," *Results in Physics*, vol. 30, p. 104802, 2021.
- [3] K. Wang, M. Kong, W. Zhou, J. Ding, and J. Yu, "200-Gbit/s PAM4 generation by a dual-polarization mach-zehnder modulator without DAC," *IEEE Photonics Technology Letters*, vol. 32, no. 18, pp. 1223-1226, 2020. <https://doi.org/10.1109/lpt.2020.3017535>
- [4] L. N. Binh, "Optical modulation: Advanced techniques and applications in transmission systems and networks," 1st ed. USA: Taylor & Francis Group, 2017, p. 681.
- [5] D. T. Le, N. M. Nguyen, and T. T. Le, "Zero-chirp and low power PAM-4 modulation based on SOI cascaded multimode interference structures," *Radioengineering*, vol. 31, no. 1, pp. 1-6, 2022. <https://doi.org/10.13164/re.2022.0001>
- [6] O. Jafari, S. Zhalehpour, W. Shi, and S. LaRochelle, "Dac-less pam-4 slow-light silicon photonic modulator providing high efficiency and stability," *Journal of Lightwave Technology*, vol. 39, no. 15, pp. 5074-5082, 2021. <https://doi.org/10.1109/jlt.2021.3083140>
- [7] J. He *et al.*, "Design of a PAM-4 VCSEL-based transceiver front-end for beyond-400G short-reach optical interconnects," *IEEE Transactions on Circuits and Systems I: Regular Papers*, vol. 69, no. 11, pp. 4345-4357, 2022. <https://doi.org/10.1109/tcsi.2022.3179678>
- [8] W. Zhang, "Silicon MOS-capacitor modulators: Scaling the modulation bandwidth, phase efficiency and compactness," presented at the In European Conference on Optical Communication (ECOC) 2022, Basel, J. H. C. O. B. Leuthold and H. Limberger, Eds., 2022/09/18 2022: Optica Publishing Group, in Technical Digest Series, p. We4E.2, 2022. Retrieved: <https://opg.optica.org/abstract.cfm?URI=ECEOC-2022-We4E.2>.
- [9] T.-H. Yen and Y.-J. Hung, "Fabrication-tolerant CWDM (de) multiplexer based on cascaded mach-zehnder interferometers on silicon-on-insulator," *Journal of Lightwave Technology*, vol. 39, no. 1, pp. 146-153, 2020. <https://doi.org/10.1109/jlt.2020.3026314>
- [10] Q. Liao *et al.*, "A 50-Gb/s PAM-4 silicon-photonic transmitter incorporating lumped-segment MZM, distributed CMOS driver, and integrated CDR," *IEEE Journal of Solid-State Circuits*, vol. 57, no. 3, pp. 767-780, 2021. <https://doi.org/10.1109/jssc.2021.3134874>
- [11] H. Li *et al.*, "A 3-D-integrated silicon photonic microring-based 112-Gb/s PAM-4 transmitter with nonlinear equalization and thermal control," *IEEE Journal of Solid-State Circuits*, vol. 56, no. 1, pp. 19-29, 2020. <https://doi.org/10.1109/jssc.2020.3022851>
- [12] D. W. Chan, X. Wu, Z. Zhang, C. Lu, A. P. T. Lau, and H. K. Tsang, "C-band 67 GHz silicon photonic microring modulator for dispersion-uncompensated 100 Gbaud PAM-4," *Optics Letters*, vol. 47, no. 11, pp. 2935-2938, 2022. <https://doi.org/10.1364/ol.460602>
- [13] S. Pal, A. Kumar, and S. Gupta, "PAM-4 generation using an electrostatic doping aided single silicon microring modulator driven by two binary electrical signals," *Optik*, vol. 231, p. 166373, 2021. <https://doi.org/10.1016/j.jlleo.2021.166373>
- [14] D. Zheng and C. Qiu, "20Gb/s PAM-4 generation by modulating A single-drive push-pull silicon dual-ring modulator with 3Vpp," presented at the In Asia Communications and Photonics Conference (ACPC) 2019, Chengdu, 2019/11/02 2019: Optica Publishing Group, in OSA Technical Digest, p. M4A.237, 2019. Retrieved: <https://opg.optica.org/abstract.cfm?URI=ACPC-2019-M4A.237>.
- [15] A. H. Talkhooncheh, "A 2.4pJ/b 100Gb/s 3D-integrated PAM-4 optical transmitter with segmented SiP MOSCAP modulators and a 2-channel 28nm CMOS driver," *In 2022 IEEE International Solid- State Circuits Conference*, vol. 65, pp. 284-286, 2022.
- [16] X. Zhenzhu, Z. Yupeng, G. Xudong, C. Jiming, C. Yuhua, and M. Li, "High-speed silicon optical modulator with a single-drive push-pull scheme," *In Proc.SPIE*, vol. 11780, pp. 1-6, 2021. <https://doi.org/10.1117/12.2590214>
- [17] W. Shi, Y. Xu, H. Sephehrian, S. LaRochelle, and L. A. Rusch, "Silicon photonic modulators for PAM transmissions," *Journal of Optics*, vol. 20, no. 8, p. 083002, 2018. <https://doi.org/10.1088/2040-8986/aacd65>
- [18] X. Guo, C.-I. Zou, C. Schuck, H. Jung, R. Cheng, and H. X. Tang, "Parametric down-conversion photon-pair source on a nanophotonic chip," *Light: Science & Applications*, vol. 6, no. 5, pp. 1-8, 2017. <https://doi.org/10.1038/lsa.2016.249>
- [19] S. K. Ray, T. Samanta, S. Guchhait, P. Mitra, R. Shunmugam, and N. Ghosh, "Fano resonance in plasmonic crystals enables high-sensitive arsenite detection," *Plasmonics*, vol. 17, no. 5, pp. 2015-2021, 2022.
- [20] K. Ma, Y. Zhang, H. Su, G. Yi, C. Yu, and Y. Wu, "Tunable Fano and EIT-like resonances in a nested feedback ring resonator," *Journal of Lightwave Technology*, vol. 40, no. 7, pp. 2040-2044, 2022. <https://doi.org/10.1109/jlt.2021.3070748>
- [21] F. Zangeneh-Nejad and R. Fleury, "Topological fano resonances," *Physical Review Letters*, vol. 122, no. 1, p. 014301, 2019. <https://doi.org/10.1103/physrevlett.122.014301>

- [22] W. Cheng *et al.*, "Achieving fano resonance with an ultra-high slope rate by silicon nitride CROW embedded in a mach-zehnder interferometer," *Optics Express*, vol. 30, no. 26, pp. 46147-46156, 2022. <https://doi.org/10.1364/oe.477261>
- [23] M. F. Limonov, "Fano resonance for applications," *Advances in Optics and Photonics*, vol. 13, no. 3, pp. 703-771, 2021. <https://doi.org/10.1364/aop.420731>
- [24] X. Liu, Y. Yu, and X. Zhang, "Tunable Fano resonance with a high slope rate in a microring-resonator-coupled mach-zehnder interferometer," *Optics Letters*, vol. 44, no. 2, pp. 251-254, 2019. <https://doi.org/10.1364/ol.44.000251>
- [25] L. Gu *et al.*, "Fano resonance lineshapes in a waveguide-microring structure enabled by an air-hole," *APL Photonics*, vol. 5, no. 1, pp. 1-8, 2020. <https://doi.org/10.1063/1.5124092>
- [26] T. Zhao *et al.*, "Independently tunable double Fano resonances based on waveguide-coupled cavities," *Optics Letters*, vol. 44, no. 12, pp. 3154-3157, 2019. <https://doi.org/10.1364/ol.44.003154>
- [27] D. A. Bekele *et al.*, "Signal reshaping and noise suppression using photonic crystal Fano structures," *Optics Express*, vol. 26, no. 15, pp. 19596-19605, 2018. <https://doi.org/10.1364/oe.26.019596>
- [28] Q. Saudan, D. A. Bekele, M. Xiong, K. Yvind, J. Mørk, and M. Galili, "All-optical switching using a photonic crystal molecule with asymmetric Fano lineshape," presented at the In European Conference on Optical Communication (ECOC) 2022, Basel, J. H. C. O. B. Leuthold and H. Limberger, Eds., 2022/09/18 2022: Optica Publishing Group, in Technical Digest Series, p. Tu5.13, 2022. Retrieved: <https://opg.optica.org/abstract.cfm?URI=ECEOC-2022-Tu5.13>.
- [29] A. Rizzo *et al.*, "Fabrication-robust silicon photonic devices in standard sub-micron silicon-on-insulator processes," *Optics Letters*, vol. 48, no. 2, pp. 215-218, 2023. <https://doi.org/10.1364/ol.476873>
- [30] H. Shahoei *et al.*, "Silicon photonics 2x2 trench coupler design and foundry fabrication," *Applied Optics*, vol. 61, no. 16, pp. 4927-4931, 2022. <https://doi.org/10.1364/ao.453464>
- [31] G. N. Tzintzarov, S. G. Rao, and J. D. Cressler, "Integrated silicon photonics for enabling next-generation space systems," *Photonics*, vol. 8, no. 4, pp. 1-19, 2021. <https://doi.org/10.3390/photonics8040131>
- [32] Y. Hao *et al.*, "Recent progress of integrated circuits and optoelectronic chips," *Science China Information Sciences*, vol. 64, no. 10, p. 201401, 2021.
- [33] A. Samani, V. Veerasubramanian, E. El-Fiky, D. Patel, and D. V. Plant, "A silicon photonic PAM-4 modulator based on dual-parallel mach-zehnder interferometers," *IEEE Photonics Journal*, vol. 8, no. 1, pp. 1-10, 2015. <https://doi.org/10.1109/jphot.2015.2512105>
- [34] R. Li *et al.*, "Silicon photonic dual-drive MIM based 56 Gb/s DAC-less and DSP-free PAM-4 transmission," *Optics Express*, vol. 26, no. 5, pp. 5395-5407, 2018. <https://doi.org/10.1364/oe.26.005395>
- [35] V. Moshaeiev, Y. Leibin, and D. Malka, "Optimizations of Si PIN diode phase-shifter for controlling MZM quadrature bias point using SOI rib waveguide technology," *Optics Laser Technology*, vol. 138, p. 106844, 2021. <https://doi.org/10.1016/j.optlastec.2020.106844>
- [36] D. M. Dourado, G. B. D. Farias, M. D. M. A. C. Moreira, M. D. L. Rocha, and J. P. Carmo, "Silicon modulator design using a system-oriented methodology for high-speed data center interconnect PAM-4 applications," *Optics Communications*, vol. 492, p. 126977, 2021. <https://doi.org/10.1016/j.optcom.2021.126977>
- [37] K. Okamoto, "Fundamentals of optical waveguides," 3rd ed. USA: Academic Press, 2021, p. 734.
- [38] J. M. Heaton and R. M. Jenkins, "General matrix theory of self-imaging in multimode interference (MMI) couplers," *IEEE Photonics Technology Letters*, vol. 11, no. 2, pp. 212-214, 1999. <https://doi.org/10.1109/68.740707>
- [39] T.-T. Le, "Two-channel highly sensitive sensors based on 4x4 multimode interference couplers," *Photonic Sensors*, vol. 7, no. 4, pp. 357-364, 2017. <https://doi.org/10.1007/s13320-017-0441-1>
- [40] T.-T. Le, *Multimode interference structures for photonic signal processing: Modeling and design*. Germany: Lambert Academic Publishing, 2010.
- [41] L. Vivien and L. Pavesi, "Handbook of silicon photonics." USA: CRC Press, 2013, p. 868.
- [42] A. Yariv, "Universal relations for coupling of optical power between microresonators and dielectric waveguides," *Electronics Letters*, vol. 36, no. 4, pp. 321-322, 2000. <https://doi.org/10.1049/el:20000340>
- [43] L. Vivien *et al.*, "Comparison between strip and rib SOI microwaveguides for intra-chip light distribution," *Optical Materials*, vol. 27, no. 5, pp. 756-762, 2005. <https://doi.org/10.1016/j.optmat.2004.08.010>
- [44] D.-T. Le, M.-C. Nguyen, and T.-T. Le, "Fast and slow light enhancement using cascaded microring resonators with the sagnac reflector," *Optik -International Journal for Light and Electron Optics*, vol. 131, pp. 292-301, 2017. <https://doi.org/10.1016/j.ijleo.2016.11.038>
- [45] R. Li *et al.*, "High-speed low-chirp PAM-4 transmission based on push-pull silicon photonic microring modulators," *Optics Express*, vol. 25, no. 12, pp. 13222-13229, 2017. <https://doi.org/10.1364/oe.25.013222>